

# World Journal of *Clinical Cases*

*World J Clin Cases* 2021 August 26; 9(24): 6964-7291



**OPINION REVIEW**

- 6964 Reconsideration of recurrence and metastasis in colorectal cancer  
*Wang R, Su Q, Yan ZP*

**MINIREVIEWS**

- 6969 Multiple immune function impairments in diabetic patients and their effects on COVID-19  
*Lu ZH, Yu WL, Sun Y*
- 6979 Discontinuation of antiviral therapy in chronic hepatitis B patients  
*Medas R, Liberal R, Macedo G*

**ORIGINAL ARTICLE****Case Control Study**

- 6987 Textural differences based on apparent diffusion coefficient maps for discriminating pT3 subclasses of rectal adenocarcinoma  
*Lu ZH, Xia KJ, Jiang H, Jiang JL, Wu M*

**Retrospective Cohort Study**

- 6999 Cost-effective screening using a two-antibody panel for detecting mismatch repair deficiency in sporadic colorectal cancer  
*Kim JB, Kim YI, Yoon YS, Kim J, Park SY, Lee JL, Kim CW, Park IJ, Lim SB, Yu CS, Kim JC*

**Retrospective Study**

- 7009 Novel model combining contrast-enhanced ultrasound with serology predicts hepatocellular carcinoma recurrence after hepatectomy  
*Tu HB, Chen LH, Huang YJ, Feng SY, Lin JL, Zeng YY*
- 7022 Influence of volar margin of the lunate fossa fragment fixation on distal radius fracture outcomes: A retrospective series  
*Meng H, Yan JZ, Wang B, Ma ZB, Kang WB, Liu BG*
- 7032 Case series of COVID-19 patients from the Qinghai-Tibetan Plateau Area in China  
*Li JJ, Zhang HQ, Li PJ, Xin ZL, Xi AQ, Zhuo-Ma, Ding YH, Yang ZP, Ma SQ*
- 7043 Patients' awareness about their own breast cancer characteristics  
*Geng C, Lu GJ, Zhu J, Li YY*
- 7053 Fracture risk assessment in children with benign bone lesions of long bones  
*Li HB, Ye WS, Shu Q*

**SYSTEMATIC REVIEWS**

- 7062 Mothers' experiences of neonatal intensive care: A systematic review and implications for clinical practice  
*Wang LL, Ma JJ, Meng HH, Zhou J*

**META-ANALYSIS**

- 7073 *Helicobacter pylori* infection and peptic ulcer disease in cirrhotic patients: An updated meta-analysis  
*Wei L, Ding HG*

**CASE REPORT**

- 7085 Tuberosus sclerosis complex-lymphangiomyomatosis involving several visceral organs: A case report  
*Chen HB, Xu XH, Yu CG, Wan MT, Feng CL, Zhao ZY, Mei DE, Chen JL*
- 7092 Long-term survivor of metastatic squamous-cell head and neck carcinoma with occult primary after cetuximab-based chemotherapy: A case report  
*Große-Thie C, Maletzki C, Junghanss C, Schmidt K*
- 7099 Genetic mutations associated with sensitivity to neoadjuvant chemotherapy in metastatic colon cancer: A case report and review of literature  
*Zhao L, Wang Q, Zhao SD, Zhou J, Jiang KW, Ye YJ, Wang S, Shen ZL*
- 7110 Coexistence of cervical extramedullary plasmacytoma and squamous cell carcinoma: A case report  
*Zhang QY, Li TC, Lin J, He LL, Liu XY*
- 7117 Reconstruction of the chest wall after resection of malignant peripheral nerve sheath tumor: A case report  
*Guo X, Wu WM, Wang L, Yang Y*
- 7123 A rare occurrence of a hereditary Birt-Hogg-Dubé syndrome: A case report  
*Lu YR, Yuan Q, Liu J, Han X, Liu M, Liu QQ, Wang YG*
- 7133 Late-onset Leigh syndrome without delayed development in China: A case report  
*Liang JM, Xin CJ, Wang GL, Wu XM*
- 7139 New mechanism of partial duplication and deletion of chromosome 8: A case report  
*Jiang Y, Tang S, He F, Yuan JX, Zhang Z*
- 7146 S-1 plus temozolomide as second-line treatment for neuroendocrine carcinoma of the breast: A case report  
*Wang X, Shi YF, Duan JH, Wang C, Tan HY*
- 7154 Minimally invasive treatment of hepatic hemangioma by transcatheter arterial embolization combined with microwave ablation: A case report  
*Wang LZ, Wang KP, Mo JG, Wang GY, Jin C, Jiang H, Feng YF*
- 7163 Progressive disfiguring facial masses with pupillary axis obstruction from Morbihan syndrome: A case report  
*Zhang L, Yan S, Pan L, Wu SF*

- 7169** Idiopathic basal ganglia calcification associated with new *MYORG* mutation site: A case report  
*Fei BN, Su HZ, Yao XP, Ding J, Wang X*
- 7175** Geleophysic dysplasia caused by a mutation in *FBNI*: A case report  
*Tao Y, Wei Q, Chen X, Nong GM*
- 7181** Combined laparoscopic-endoscopic approach for gastric glomus tumor: A case report  
*Wang WH, Shen TT, Gao ZX, Zhang X, Zhai ZH, Li YL*
- 7189** Aspirin-induced long-term tumor remission in hepatocellular carcinoma with adenomatous polyposis coli stop-gain mutation: A case report  
*Lin Q, Bai MJ, Wang HF, Wu XY, Huang MS, Li X*
- 7196** Prenatal diagnosis of isolated lateral facial cleft by ultrasonography and three-dimensional printing: A case report  
*Song WL, Ma HO, Nan Y, Li YJ, Qi N, Zhang LY, Xu X, Wang YY*
- 7205** Therapy-related myeloid leukemia during erlotinib treatment in a non-small cell lung cancer patient: A case report  
*Koo SM, Kim KU, Kim YK, Uh ST*
- 7212** Pediatric schwannoma of the tongue: A case report and review of literature  
*Yun CB, Kim YM, Choi JS, Kim JW*
- 7218** Status epilepticus as a complication after COVID-19 mRNA-1273 vaccine: A case report  
*Šin R, Štruncová D*
- 7224** Successful outcome of retrograde pancreatojejunostomy for chronic pancreatitis and infected pancreatic cysts: A case report  
*Kimura K, Adachi E, Toyohara A, Omori S, Ezaki K, Ihara R, Higashi T, Ohgaki K, Ito S, Maehara SI, Nakamura T, Maehara Y*
- 7231** Incidentally discovered asymptomatic splenic hamartoma misdiagnosed as an aneurysm: A case report  
*Cao XF, Yang LP, Fan SS, Wei Q, Lin XT, Zhang XY, Kong LQ*
- 7237** Secondary peripheral T-cell lymphoma and acute myeloid leukemia after Burkitt lymphoma treatment: A case report  
*Huang L, Meng C, Liu D, Fu XJ*
- 7245** Retroperitoneal bronchogenic cyst in suprarenal region treated by laparoscopic resection: A case report  
*Wu LD, Wen K, Cheng ZR, Alwalid O, Han P*
- 7251** Coexistent vestibular schwannoma and meningioma in a patient without neurofibromatosis: A case report and review of literature  
*Zhao LY, Jiang YN, Wang YB, Bai Y, Sun Y, Li YQ*
- 7261** Thoracoabdominal duplication with hematochezia as an onset symptom in a baby: A case report  
*Yang SB, Yang H, Zheng S, Chen G*

- 7269 Dental management of a patient with Moebius syndrome: A case report  
*Chen B, Li LX, Zhou LL*
- 7279 Epidural gas-containing pseudocyst leading to lumbar radiculopathy: A case report  
*Chen Y, Yu SD, Lu WZ, Ran JW, Yu KX*
- 7285 Regression of intervertebral disc calcification combined with ossification of the posterior longitudinal ligament: A case report  
*Wang XD, Su XJ, Chen YK, Wang WG*

**ABOUT COVER**

Editorial Board Member of *World Journal of Clinical Cases*, Vijaykumar Chava, MD, Professor, Department of Periodontology, Narayana Dental College and Hospital, Nellore 524003, Andhra Pradesh, India.  
chava7@hotmail.com

**AIMS AND SCOPE**

The primary aim of *World Journal of Clinical Cases* (*WJCC*, *World J Clin Cases*) is to provide scholars and readers from various fields of clinical medicine with a platform to publish high-quality clinical research articles and communicate their research findings online.

*WJCC* mainly publishes articles reporting research results and findings obtained in the field of clinical medicine and covering a wide range of topics, including case control studies, retrospective cohort studies, retrospective studies, clinical trials studies, observational studies, prospective studies, randomized controlled trials, randomized clinical trials, systematic reviews, meta-analysis, and case reports.

**INDEXING/ABSTRACTING**

The *WJCC* is now indexed in Science Citation Index Expanded (also known as SciSearch®), Journal Citation Reports/Science Edition, Scopus, PubMed, and PubMed Central. The 2021 Edition of Journal Citation Reports® cites the 2020 impact factor (IF) for *WJCC* as 1.337; IF without journal self cites: 1.301; 5-year IF: 1.742; Journal Citation Indicator: 0.33; Ranking: 119 among 169 journals in medicine, general and internal; and Quartile category: Q3. The *WJCC*'s CiteScore for 2020 is 0.8 and Scopus CiteScore rank 2020: General Medicine is 493/793.

**RESPONSIBLE EDITORS FOR THIS ISSUE**

Production Editor: *Ji-Hong Lin*, Production Department Director: *Yn-Jie Ma*, Editorial Office Director: *Jin-Lei Wang*.

**NAME OF JOURNAL**

*World Journal of Clinical Cases*

**ISSN**

ISSN 2307-8960 (online)

**LAUNCH DATE**

April 16, 2013

**FREQUENCY**

Thrice Monthly

**EDITORS-IN-CHIEF**

Dennis A Bloomfield, Sandro Vento, Bao-Gan Peng

**EDITORIAL BOARD MEMBERS**

<https://www.wjgnet.com/2307-8960/editorialboard.htm>

**PUBLICATION DATE**

August 26, 2021

**COPYRIGHT**

© 2021 Baishideng Publishing Group Inc

**INSTRUCTIONS TO AUTHORS**

<https://www.wjgnet.com/bpg/gerinfo/204>

**GUIDELINES FOR ETHICS DOCUMENTS**

<https://www.wjgnet.com/bpg/GerInfo/287>

**GUIDELINES FOR NON-NATIVE SPEAKERS OF ENGLISH**

<https://www.wjgnet.com/bpg/gerinfo/240>

**PUBLICATION ETHICS**

<https://www.wjgnet.com/bpg/GerInfo/288>

**PUBLICATION MISCONDUCT**

<https://www.wjgnet.com/bpg/gerinfo/208>

**ARTICLE PROCESSING CHARGE**

<https://www.wjgnet.com/bpg/gerinfo/242>

**STEPS FOR SUBMITTING MANUSCRIPTS**

<https://www.wjgnet.com/bpg/GerInfo/239>

**ONLINE SUBMISSION**

<https://www.f6publishing.com>

## Case Control Study

# Textural differences based on apparent diffusion coefficient maps for discriminating pT3 subclasses of rectal adenocarcinoma

Zhi-Hua Lu, Kai-Jian Xia, Heng Jiang, Jian-Long Jiang, Mei Wu

**ORCID number:** Zhi-Hua Lu 0000-0002-6860-1449; Kai-Jian Xia 0000-0002-3180-0903; Heng Jiang 0000-0002-9713-9011; Jian-Long Jiang 0000-0002-1321-3019; Mei Wu 0000-0001-9029-9349.

**Author contributions:** Lu ZH conceived and coordinated the study, designed, performed, and analyzed the experiments, and wrote the paper; Xia KJ, Jiang H, Jiang JL, and Wu M carried out the data collection and analysis, and revised the paper; all authors reviewed the results and approved the final version of the manuscript.

**Supported by** Jiangsu Provincial Medical Youth Talent, No. QNRC2016212; Suzhou Clinical Special Disease Diagnosis and Treatment Program, No. LCZX201823; Suzhou GuSu Medical Talent Project, No. GSWS2019077; The Science and Technology Bureau of Changshu, No. CS201624 (to Lu ZH); and Jiangsu Committee of Health, No. H2018071 (to Xia KJ).

**Institutional review board**

**statement:** This case-control study was approved by the Institutional Review Board of the Changshu Hospital Affiliated to Soochow University (2018 Ethics Audit (Declaration) Batch No. 3).

**Zhi-Hua Lu, Heng Jiang,** Department of Radiology, Changshu Hospital Affiliated to Soochow University, Changshu No. 1 People's Hospital, Changshu 215500, Jiangsu Province, China

**Kai-Jian Xia,** Department of Information, Changshu Hospital Affiliated to Soochow University, Changshu No. 1 People's Hospital, Changshu 215500, Jiangsu Province, China

**Jian-Long Jiang,** Department of Surgery, Changshu Hospital Affiliated to Soochow University, Changshu No. 1 People's Hospital, Changshu 215500, Jiangsu Province, China

**Mei Wu,** Department of Pathology, Changshu Hospital Affiliated to Soochow University, Changshu No. 1 People's Hospital, Changshu 215500, Jiangsu Province, China

**Corresponding author:** Zhi-Hua Lu, MD, Doctor, Department of Radiology, Changshu Hospital Affiliated to Soochow University, Changshu No. 1 People's Hospital, No. 1 Shuyuan Street, Changshu 215500, Jiangsu Province, China. [luzhijia79@163.com](mailto:luzhijia79@163.com)

## Abstract

### BACKGROUND

The accuracy of discriminating pT3a from pT3b-c rectal cancer using high-resolution magnetic resonance imaging (MRI) remains unsatisfactory, although texture analysis (TA) could improve such discrimination.

### AIM

To investigate the value of TA on apparent diffusion coefficient (ADC) maps in differentiating pT3a rectal adenocarcinomas from pT3b-c tumors.

### METHODS

This was a case-control study of 59 patients with pT3 rectal adenocarcinoma, who underwent diffusion-weighted imaging (DWI) between October 2016 and December 2018. The inclusion criteria were: (1) Proven pT3 rectal adenocarcinoma; (2) Primary MRI including high-resolution T2-weighted image (T2WI) and DWI; and (3) Availability of pathological reports for surgical specimens. The exclusion criteria were: (1) Poor image quality; (2) Preoperative chemoradiation therapy; and (3) A different pathological type. First-order (ADC values, skewness, kurtosis, and uniformity) and second-order (energy, entropy, inertia, and correlation) texture features were derived from whole-lesion ADC maps. Receiver operating characteristic curves were used to determine the diagnostic value for pT3b-c tumors.

**Informed consent statement:** The requirement for individual informed consent was waived because of the retrospective design of the study.

**Conflict-of-interest statement:** No benefits in any form have been received or will be received from a commercial party related directly or indirectly to the subject of this article.

**Data sharing statement:** The datasets used and/or analyzed during the current study are available from the corresponding author on reasonable request.

**STROBE statement:** The authors have read the STROBE Statement – checklist of items, and the manuscript was prepared and revised according to the STROBE Statement – checklist of items.

**Open-Access:** This article is an open-access article that was selected by an in-house editor and fully peer-reviewed by external reviewers. It is distributed in accordance with the Creative Commons Attribution NonCommercial (CC BY-NC 4.0) license, which permits others to distribute, remix, adapt, build upon this work non-commercially, and license their derivative works on different terms, provided the original work is properly cited and the use is non-commercial. See: <http://creativecommons.org/licenses/by-nc/4.0/>

**Manuscript source:** Unsolicited manuscript

**Specialty type:** Oncology

**Country/Territory of origin:** China

**Peer-review report's scientific quality classification**

Grade A (Excellent): 0  
Grade B (Very good): 0  
Grade C (Good): C  
Grade D (Fair): 0  
Grade E (Poor): 0

**Received:** January 1, 2021

**Peer-review started:** January 1, 2021

**First decision:** January 24, 2021

## RESULTS

The final study population consisted of 59 patients (34 men and 25 women), with a median age of 66 years (range, 41-85 years). Thirty patients had pT3a, 24 had pT3b, and five had pT3c. Among the ADC first-order textural differences between pT3a and pT3b-c rectal adenocarcinomas, only skewness was significantly lower in the pT3a tumors than in pT3b-c tumors. Among the ADC second-order textural differences, energy and entropy were significantly different between pT3a and pT3b-c rectal adenocarcinomas. For differentiating pT3a rectal adenocarcinomas from pT3b-c tumors, the areas under the curves (AUCs) of skewness, energy, and entropy were 0.686, 0.657, and 0.747, respectively. Logistic regression analysis of all three features yielded a greater AUC (0.775) in differentiating pT3a rectal adenocarcinomas from pT3b-c tumors (69.0% sensitivity and 83.3% specificity).

## CONCLUSION

TA features derived from ADC maps might potentially differentiate pT3a rectal adenocarcinomas from pT3b-c tumors.

**Key Words:** Diffusion-weighted imaging; Apparent diffusion coefficient; Rectal cancer; Cancer stage; Texture analysis; case-control study

©The Author(s) 2021. Published by Baishideng Publishing Group Inc. All rights reserved.

**Core Tip:** Texture features derived from apparent diffusion coefficient maps might potentially differentiate pT3a rectal adenocarcinomas from pT3b-c tumors.

**Citation:** Lu ZH, Xia KJ, Jiang H, Jiang JL, Wu M. Textural differences based on apparent diffusion coefficient maps for discriminating pT3 subclasses of rectal adenocarcinoma. *World J Clin Cases* 2021; 9(24): 6987-6998

**URL:** <https://www.wjgnet.com/2307-8960/full/v9/i24/6987.htm>

**DOI:** <https://dx.doi.org/10.12998/wjcc.v9.i24.6987>

## INTRODUCTION

Colorectal cancer, the third commonest malignancy around the world, most commonly affects elderly individuals  $\geq 60$  years old, with a male predominance[1-3]. The incidence of rectal cancer was 5.2 per 100000 in 2014[4]. The 5-year relative survival is 37%-100% for local disease (varying widely according to perineural invasion and satellite nodules), 44% for locoregional disease, and 8%-15% for metastatic disease[5].

The majority (60%-80%) of rectal tumors are in the pT3 stage at diagnosis, constituting a heterogeneous group[6,7]. The extramural depth (EMD) of tumor invasion is one of the most important prognostic factors in rectal cancer, and strongly influences survival and local recurrence[6]. The 5-mm cut-off of EMD has been determined to be the most discriminating and simple to use in clinical practice regardless of differences in overall survival (OS) and local recurrence[6-9]. Locoregional recurrence and cancer-related 5-year survival rates are 10.4% and 85.4% for pT3a (EMD < 5 mm), respectively, and 26.3% and 54.1% for pT3b (EMD  $\geq 5$  mm), respectively[9]. Therefore, there is a need for a preoperative imaging method to noninvasively identify patients with high-risk pT3 in order to provide individualized treatment strategies.

Magnetic resonance imaging (MRI) with a phased-array surface coil has an undeniable role in the preoperative staging of rectal cancer. In preoperative local T staging, the reported overall accuracy of MRI is 71%-90%[10-13]. In two studies on pT3 subclassification, the accuracies of MRI were 71.2% and 86%[10,12]. However, the accuracy of staging using high-resolution MRI remains unsatisfactory. In recent years, the potential of MRI has extended from morphological assessments to texture analysis (TA). TA refers to various mathematical-statistical methods used to extract texture features by evaluating the spatial variation of gray levels within given images[14]. These features can be used to characterize and measure tissue heterogeneity in medical images. Some texture features are useful tools for accurate diagnosis, preoperative risk stratification, and assessment of treatment response in several cancers[15-18]. Previous

**Revised:** March 1, 2021  
**Accepted:** July 6, 2021  
**Article in press:** July 6, 2021  
**Published online:** August 26, 2021

**P-Reviewer:** Nespoli L  
**S-Editor:** Gong ZM  
**L-Editor:** Wang TQ  
**P-Editor:** Li JH



studies have demonstrated that MRI-based texture features are efficient in identifying preoperative KRAS mutation status in rectal cancer cases[19,20]. In addition, several MRI features and TA were shown to be valuable for predicting the therapeutic response to neoadjuvant chemoradiotherapy (nCRT) for rectal cancer and tumor recurrence[21]. However, another study reported that MRI T2-weighted sequence-based TA is not effective in predicting pathological complete response to nCRT in patients with locally advanced rectal cancer, suggesting that additional trials are required for comprehensively analyzing the potential of MRI-derived TA in this setting[22].

Diffusion-weighted imaging (DWI) is important in rectal cancer imaging because it provides superior contrast between cancerous and non-cancerous tissues. In a previous study[11], DWI was shown to be useful for evaluating the pT stage of rectal cancer and guiding EMD measurement. In addition, the apparent diffusion coefficient (ADC), a quantitative value of DWI, has been reported to correlate with the pT stage [11,23]. Nevertheless, the mean and median ADC values are not always significantly sensitive to small changes or precise status of the tumor owing to the intrinsic chaotic environment of tumors[24]. In addition, pT3 subclasses of rectal cancer have not been previously determined by ADC maps.

Given the increasing use of DWI in rectal cancer imaging and the quantitative value of ADC for accurate diagnosis, we hypothesized that texture features derived from ADC maps could discriminate pT3 subclasses. Therefore, the aim of this study was to investigate the value of TA on ADC maps in differentiating pT3a rectal adenocarcinomas from pT3b-c tumors. The results could provide interesting features for the tailoring of treatment strategies.

## MATERIALS AND METHODS

### Study design and patients

This case-control study was approved by the Institutional Review Board of the Changshu Hospital Affiliated to Soochow University (2018 Ethics Audit (Declaration) Batch No. 3). The requirement for individual informed consent was waived because of the retrospective design of the study. The patients who underwent imaging at the Changshu Hospital Affiliated to Soochow University between October 2016 and December 2018 were included ( $n = 120$ ).

The inclusion criteria were: (1) Proven pT3 rectal adenocarcinoma; (2) Primary MRI including high-resolution T2-weighted image (T2WI) and DWI; and (3) Availability of pathological reports of surgical specimens. A total of 67 patients met these criteria. Eight patients were excluded for the following reasons: (1) Poor image quality apparent on DWI ( $n = 2$ ); (2) Treatment with preoperative chemoradiation therapy ( $n = 4$ ); and (3) A different pathological type, such as mucinous adenocarcinoma ( $n = 2$ ).

### Data collection

Patient features (age and sex), pathological characteristics (grade and stage), and DWI TA features (ADC, skewness, kurtosis, uniformity, energy, entropy, inertia, and correlation) were collected from the medical charts.

### MRI

All patients were imaged using a 3.0-T MRI system (Intera Achieva 3.0T TX, Philips Medical System, Best, The Netherlands) and a 16-channel phased-array surface coil. Thirty minutes before the MRI examination, all patients were asked to take clyster in order to reduce artifacts caused by gas within the rectum. The patients also received 10 mg of anisodamine (Hangzhou Mingsheng Pharmaceuticals Co., Ltd., Zhejiang, China) by intramuscular injection 10 min before the examination to reduce bowel peristalsis.

The standard rectal imaging protocol consisted of sagittal T2WI turbo spin-echo (TSE) [repetition time/echo time (TR/TE), 3577/70 ms; TSE factor, 20; slice thickness, 3 mm; interspace, 0 mm; field of view (FOV), 24 cm] and high-resolution axial and coronal T2W (TR/TE, 3000/75 ms; TSE factor, 18; slice thickness, 2 mm for coronal and 3 mm for axial; interspace, 0 mm; FOV: 18 cm). Axial T2WI was perpendicular to the tumor axis, as identified on sagittal T2WI. Coronal T2WI was angled parallel to the tumor axis. In addition, axial DWI was used (TR/TE, 2750/76 ms; slice thickness, 3 mm; interspace, 0 mm; FOV, 22-24 cm; b-values, 0, 1000 s/mm<sup>2</sup>). Dynamic contrast-enhanced imaging was not assessed in this study. ADC maps were automatically generated from DWI data using a mono-exponential decay model.

### **Image analysis and textural features calculation**

The primary tumor was distinguished on high-resolution T2WI and DWI based on final pathological outcomes. The primary tumor site was determined as a focal mass or abnormal wall thickening with intermediate signal intensity on T2WI, hyperintensity on DWI ( $b$  value = 1000 s/mm<sup>2</sup>), and the corresponding hypointensity on grey-scale ADC map. The entire tumor volumes were segmented independently by two experienced radiologists (Z.L. and H.J., with 9 and 4 years of experience in gastrointestinal MRI, respectively), using the Omni-Kinetics software (GE Healthcare, Waukesha, WI, United States). The resulting ADC maps were imported into Omni-Kinetics. The regions of interest (ROIs) were manually drawn slice by slice just inside the outer margin of the lesion to minimize partial volume error. The entire tumor area was covered as much as possible on ADC maps with reference to T2WI and DWI. Areas of necrosis, cysts, and gas were avoided to minimize bias. All ROIs were selected to derive the volume of interest (VOI). Then, first- and second-order texture features based on ADC maps were calculated automatically. ADC first-order texture features, as histogram features, included mean value, ADC percentiles (5<sup>th</sup>, 10<sup>th</sup>, 25<sup>th</sup>, and 90<sup>th</sup> percentiles), skewness, kurtosis, and uniformity. The ADC second-order texture features were derived from the gray-level co-occurrence matrix (GLCM), and included energy, entropy, inertia, and correlation.

### **Histopathologic extramural depth of tumor invasion**

The mean time between MRI and surgery was  $3.6 \pm 1.4$  d (range, 2-7 d). One pathologist (M.W., 15 years of experience) measured the EMD of tumor invasion on histopathologic specimens (stained routinely with hematoxylin and eosin) according to the criteria of The Radiologic Society of North America (RSNA)[7]. EMD was defined as the maximum depth of the extramural tumor spreading outside the muscularis propria (pT3a, < 5 mm; pT3b, 5-10 mm; pT3c, > 10 mm)[7]. The pathologist measured the distance between the outer border of the identifiable muscularis propria layer and the outermost border of the tumor. If the outer border was not clear, then the pathologist checked the outer border at both ends of the tumor to determine clear areas, and drew a tentative line designating the outer border of the muscle layer.

### **Statistical analysis**

Statistical analyses were performed using SPSS 16.0 (IBM, Armonk, NY, United States) and MedCalc 9.0 (MedCalc Software, Mariakierke, Belgium).  $P$  values < 0.05 were considered statistically significant. The KolmogorovSmirnov test was used to determine the distribution of all continuous data. Normally distributed data are presented as the mean  $\pm$  SD, while those with a skewed distribution are presented as the median and interquartile range. ADC texture features were compared between the pT3a and pT3b-c stages by independent samples Student's  $t$ -test or the Mann-Whitney  $U$ -test. Receiver operating characteristic (ROC) analysis was used to assess the diagnostic value of each statistically significant feature for the detection of pT3a tumors as previously proposed[25]. The areas under the curves (AUCs) were compared using the method of DeLong *et al*[26]. Interobserver variability of ADC texture features extraction was evaluated using intra-class correlation coefficients (ICCs) as follows: 0.00-0.20, poor agreement; 0.21-0.40, fair agreement; 0.41-0.60, moderate agreement; 0.61-0.80, good agreement; and 0.81-1.00, excellent agreement.

## **RESULTS**

### **Characteristics of the patients**

A summary of the baseline characteristics of the patients is shown in Table 1. The final study population consisted of 59 patients (34 men and 25 women), with a median age of 66 years (range, 41-85 years). According to the histological measurement of the maximal tumor invasion beyond the outer border of the muscularis propria, there were 30 patients with pT3a (Figure 1), 24 with pT3b (Figure 2), and five with pT3c. Twenty-seven patients were staged as N0, 22 as N1, and 10 as N2. Fifty-five patients were staged as M0, and four as M1. Forty-four patients had moderately differentiated tumors, and 15 had poorly differentiated ones.

### **ADC textural differences between pT3a and pT3b-c stages**

The ADC first-order textural differences between pT3a and pT3b-c rectal adenocarcinomas are shown in Table 2. Skewness was significantly lower in pT3a tumors than

**Table 1 Demographic and pathologic characteristics of patients**

Characteristic	<i>n</i> = 59
Age (yr), median (IQR)	66 (58-74)
Sex	
Men	34 (57.6)
Women	25 (42.4)
Differentiation grade	
Moderately differentiated	44 (74.6)
Poorly differentiated	15 (25.4)
T3 stage	
T3a	30 (50.9)
T3b	24 (40.7)
T3c	5 (8.5)
N stage	
N0	27 (45.8)
N1	22 (37.3)
N2	10 (17.0)
M stage	
M0	55 (93.2)
M1	4 (6.8)

Except for age, data are expressed as *n* (%). IQR: Interquartile range.

**Table 2 Comparison of apparent diffusion coefficient first-order textural differences between pT3a and pT3b-c stage**

ADC histogram feature	pT3a ( <i>n</i> = 30)	pT3b-c ( <i>n</i> = 29)	<i>P</i> value	ICC
Mean ADC ( $\times 10^{-6}$ mm <sup>2</sup> /s) <sup>1</sup>	879.5 $\pm$ 202.3	832.8 $\pm$ 166.7	0.339	0.906
5 <sup>th</sup> ADC ( $\times 10^{-6}$ mm <sup>2</sup> /s) <sup>1</sup>	584.4 $\pm$ 163.3	533.1 $\pm$ 111.9	0.164	0.898
10 <sup>th</sup> ADC ( $\times 10^{-6}$ mm <sup>2</sup> /s) <sup>1</sup>	638.6 $\pm$ 164.2	589.5 $\pm$ 111.0	0.183	0.901
25 <sup>th</sup> ADC ( $\times 10^{-6}$ mm <sup>2</sup> /s) <sup>1</sup>	720.2 $\pm$ 175.8	664.5 $\pm$ 125.7	0.168	0.921
90 <sup>th</sup> ADC ( $\times 10^{-6}$ mm <sup>2</sup> /s) <sup>1</sup>	1113.8 $\pm$ 275.8	1055.7 $\pm$ 229.3	0.383	0.850
Skewness <sup>1</sup>	0.24 $\pm$ 0.31	0.41 $\pm$ 0.32	0.033	0.925
Kurtosis <sup>1</sup>	0.66 $\pm$ 0.52	0.80 $\pm$ 0.70	0.376	0.909
Uniformity <sup>1</sup>	0.78 $\pm$ 0.06	0.76 $\pm$ 0.05	0.058	0.921

<sup>1</sup>Independent samples *t*-test, and data are the mean  $\pm$  SD.

ADC: Apparent diffusion coefficient; ICC: Intraclass correlation coefficient.

in pT3b-c counterparts (0.24  $\pm$  0.31 *vs* 0.41  $\pm$  0.32, *P* = 0.033). ADC value (including mean and percentiles) and ADC histogram related features (including kurtosis and uniformity) were not significantly different between the pT3a and pT3b-c stages. All ADC first-order texture features derived from ADC maps were delineated independently by two radiologists, and showed excellent agreement (ICCs ranging from 0.850 to 0.925).

The obtained ADC second-order textural differences between pT3a and pT3b-c rectal adenocarcinomas are shown in Table 3. Energy (median, 0.782 *vs* 0.640, *P* = 0.038) and entropy (median, 9.831 *vs* 10.805, *P* = 0.001) were significantly different between pT3a and pT3b-c rectal adenocarcinomas. Specifically, energy was higher for

**Table 3 Comparison of apparent diffusion coefficient textural differences between pT3a and pT3b-c stages**

ADC texture feature	pT3a (n = 30)	pT3b-c (n = 29)	P value	ICC
Energy ( $\times 10^{-3}$ ) <sup>2</sup>	0.782 (0.527, 1.399)	0.640 (0.437, 0.779)	0.038	0.895
Entropy <sup>2</sup>	9.831 (8.969, 10.652)	10.805 (10.189, 11.592)	0.001	0.920
Inertia <sup>1</sup>	753.0 $\pm$ 417.0	878.9 $\pm$ 279.0	0.180	0.918
Correlation ( $\times 10^{-3}$ ) <sup>2</sup>	0.538 (0.399, 1.255)	0.476 (0.414, 0.642)	0.332	0.921

<sup>1</sup>Independent samples *t*-test, and data are the mean  $\pm$  SD.

<sup>2</sup>Mann-Whitney *U*-test, and data are the median  $\pm$  interquartile range.

ADC: Apparent diffusion coefficient; ICC: Intra-class correlation coefficient.

pT3a tumors than for pT3b-c ones, while entropy was lower for the pT3a stage than for pT3b-c tumors. All ADC second-order texture features derived from ADC maps were delineated independently by two radiologists, and showed excellent agreement (ICCs ranging from 0.895 to 0.921).

### **Diagnostic performance of ADC first- and second-order texture features**

The diagnostic performances of statistically significant ADC first- and second-order texture features and logistic features using ROC analysis to determine the pT3a stage are shown in Table 4. For differentiating pT3a rectal adenocarcinomas from pT3b-c tumors, the AUCs of skewness, energy, and entropy were 0.686, 0.657, and 0.747, respectively. Using a logistic regression model that incorporated all three texture parameters, a moderate accuracy (AUC, 0.775) was achieved, with a sensitivity of 69.0% and specificity of 83.3% (Figure 3). We noted no significant AUC differences while comparing all pairs of texture parameters.

## **DISCUSSION**

In this study, we investigated the feasibility of differentiating pT3a rectal adenocarcinomas from pT3b-c tumors using first- and second-order texture features derived from ADC maps. Skewness, energy, and entropy could significantly differentiate pT3a from pT3b-c rectal adenocarcinomas. Logistic regression analysis using all three features demonstrated a higher AUC in differentiating pT3a from pT3b-c tumors. The results indicate that texture features derived from ADC maps might potentially differentiate pT3a from pT3b-c rectal adenocarcinomas.

Statistics-based techniques are the most commonly used methods for TA[27] and contain three orders of features. First-order statistics can be obtained from the histogram of pixel intensity values, including mean intensity, maximum intensity, minimum intensity, standard deviation, uniformity, skewness, and kurtosis. Among second-order statistics, GLCM measurements calculated using spatial gray-level dependence matrices are well known, and these parameters also describe the relationship between neighboring pixels[28,29], including energy, entropy, total frequency, matrix mean, inertia, and correlation. Third-order statistics show the spatial relationships among three or more pixels[28,29]. In this study, ADC histogram features were based on first-order statistics, and GLCM measurements were based on second-order statistics.

In previous studies, the mean ADC values were significantly different among rectal cancers with different pT3 subclasses[23]. In the current study, mean ADC values were not statistically different between pT3a and pT3b-c tumors. Such a discrepancy could result from the methods used for calculating ADC. In the studies by Lu *et al*[11] and Tong *et al*[23], mean ADC values were calculated from three round ROIs that were manually delineated within solid tumor parts. On the contrary, we used whole-tumor VOI, which might better reflect the heterogeneity of the whole tumor[24]. In previous studies by our group[30,31], the 10th percentile ADC from the histogram performed better in differentiating the transition zone cancer from benign prostatic hyperplasia nodule, and was best correlated with the Gleason score of prostate cancer, because the low proportion (*e.g.*, minimum, 10th percentile) ADC from the histogram represents the focal areas of high cellularity under the heterogeneous background[32]. Therefore, we hypothesized that the low proportion of ADC from the histogram could differ-

**Table 4 Diagnostic performances of texture features and logistic feature to discriminate pT3a rectal adenocarcinomas from pT3b-c tumors**

Texture features	AUC (95%CI)	Sensitivity	Specificity	+LR	-LR	+PV	-PV	Comparison of AUC (P value)			
								Skewness	Energy	Entropy	Logistic feature
Skewness	0.686 (0.552-0.801)	75.9%	63.3%	2.07	0.38	66.7	73.1	—	0.7469	0.4667	0.1471
Energy	0.657 (0.522-0.776)	86.2%	43.3%	1.52	0.32	59.5	76.2	—	0.0956	0.0617	
Entropy	0.747 (0.617-0.851)	75.9%	63.3%	2.07	0.38	66.7	73.1		—	0.3998	
Logistic feature	0.775 (0.647-0.873)	69.0%	83.3%	4.14	0.37	80.0	73.5			—	

AUC: Area under the curve; CI: Confidence interval; LR: Likelihood ratio; PV: Predictive value.

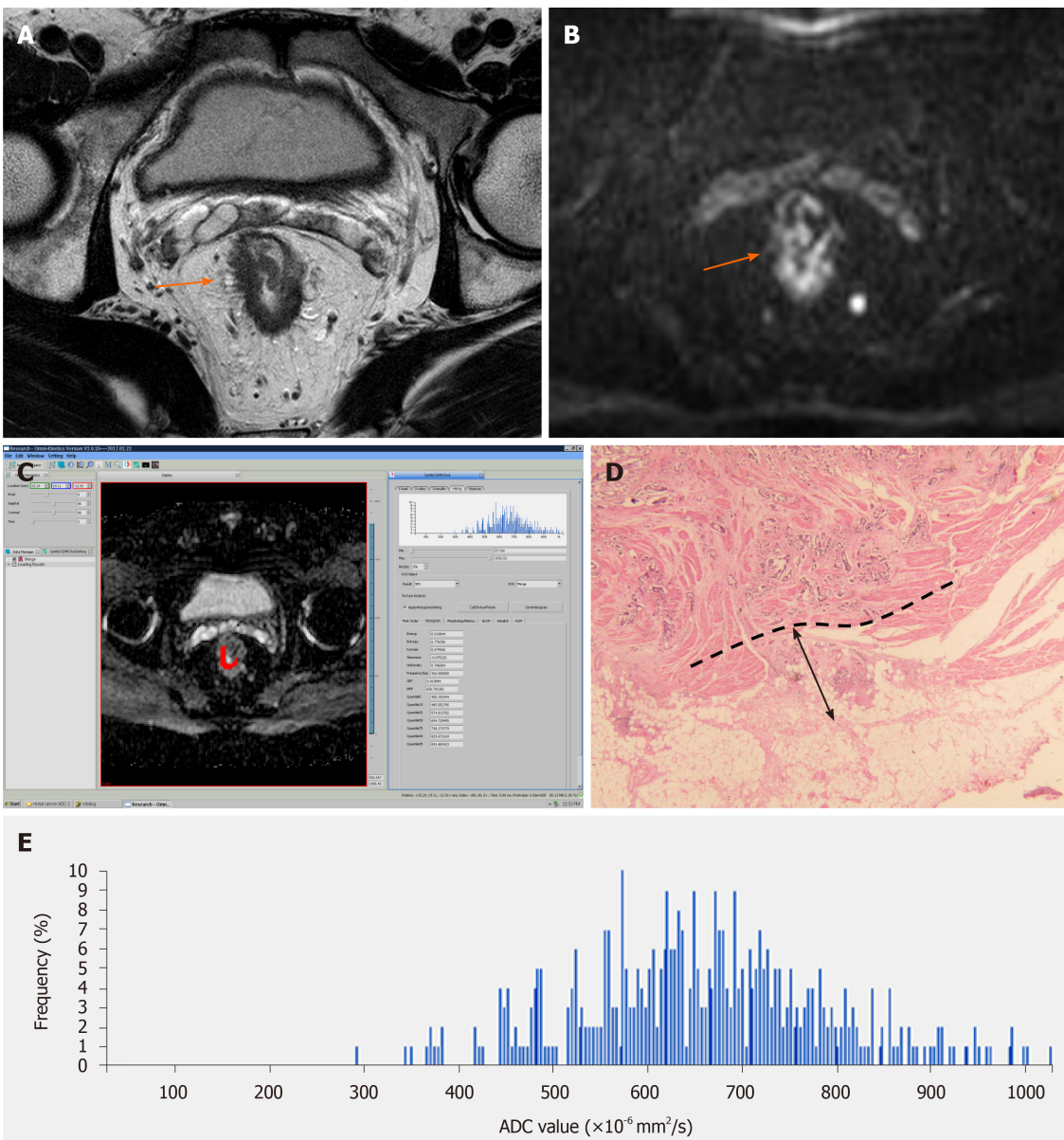


**Figure 1 T3a stage rectal adenocarcinoma.** A: Axial high-resolution T2WI showing that the rectal mass had destroyed the muscularis propria and spread into the mesorectum (orange arrow); B: Diffusion-weighted imaging showing an area of high signal intensity with irregular rectal wall margin (orange arrow); C: Regions of interest were manually drawn, slice by slice, covering the whole lesion (red area) on the apparent diffusion coefficient (ADC) map; D: Photomicrograph (hematoxylin & eosin staining, magnification  $\times 200$ ) showing that the extramural depth of tumor invasion was 2.5 mm; E: The histogram obtained from the whole lesion on ADC maps provided first-order texture features. ADC: Apparent diffusion coefficient.

entiate pT3a rectal adenocarcinomas from pT3b-c tumors. Nevertheless, the results

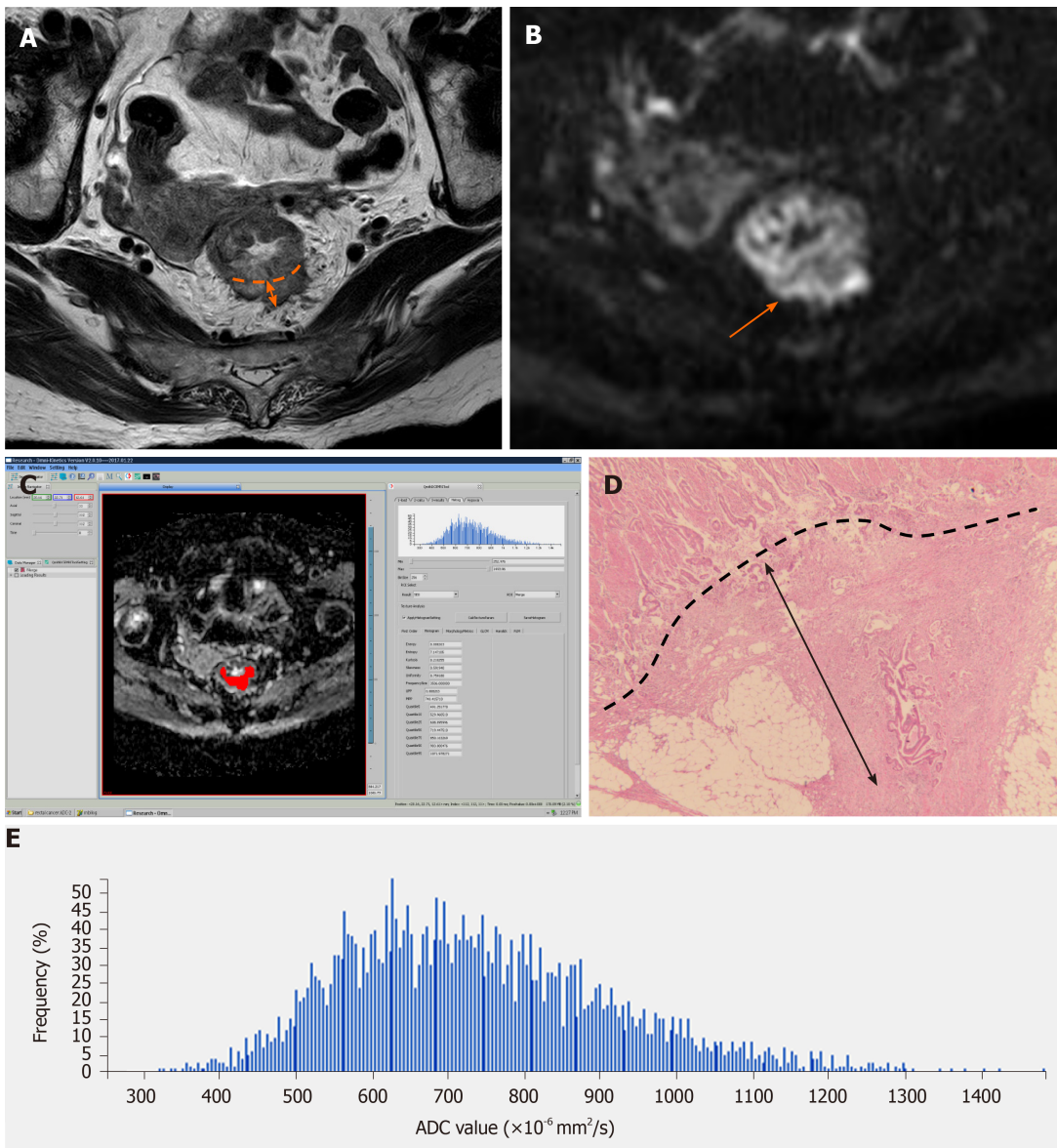


**Figure 2 T3b stage rectal adenocarcinoma.** A: Axial high-resolution T2WI showing that the muscularis propria at the 4-6 o'clock direction was destroyed. An imaginary line (dash line) connecting two breakpoints of the muscularis propria layer is shown. The tumor had spread into the mesorectum (orange double arrow); B: Diffusion-weighted imaging showing an area of high signal intensity where the tumor invaded the muscularis propria, and the 4-6 o'clock direction of the tumor was the main invasion direction (orange arrow); C: Regions of interest were manually drawn, slice by slice, covering the whole lesion (red area) on the apparent diffusion coefficient (ADC) map; D: Photomicrograph (hematoxylin & eosin staining, magnification  $\times 200$ ) showing that the extramural depth of tumor invasion was 7 mm; E: The histogram obtained from the whole lesion on ADC maps provided first-order texture features. ADC: Apparent diffusion coefficient.

showed that different percentile ADCs from the histogram were not statistically different between pT3a and pT3b-c tumors, suggesting that in rectal cancer, the pT3 stage is possibly more spatially homogeneous. In addition, the relatively small number of patients in the present study might have been a contributing factor.

As shown above, the pT3b-c stage was associated with higher skewness than the pT3a stage. Skewness reflects the asymmetry of pixel distribution. Positive skewness means that the distribution of the histogram has an elongated tail on the right side of the mean[24]. Higher skewness indicates elevated complexity and heterogeneity in tumors. This may be important when interpreting the finding that pT3b-c stage tumors have greater skewness than pT3a ones. The results of the present study were similar to those of Liu *et al*[33]. Moreover, uniformity had a near-significant difference between pT3a and pT3b-c tumors. Uniformity reflects how close the image is to a uniform distribution of gray levels, and high uniformity indicates uniformity in the image and lower heterogeneity[29]. Meng *et al*[34] reported a significant difference in pre-uniformity between advanced patients with rectal cancer that were responders *vs* non-responders in pathologic complete response. The above results revealed that uniformity was potentially advantageous in differentiating pT3a rectal adenocar-

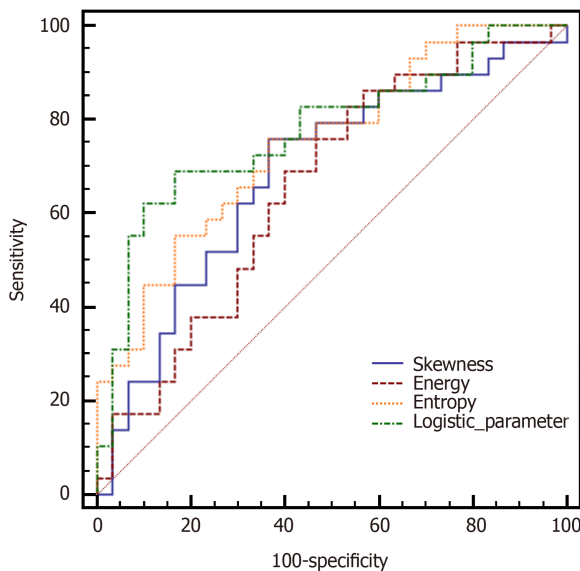


**Figure 3** Receiver operating characteristic curves of four important texture features for calculating the areas under the curves in differentiating pT3a rectal adenocarcinomas from pT3b-c tumors.

cinomas from pT3b-c tumors. Hence, future studies will need larger patient cohorts to investigate the differences in uniformity between patients with pT3a and pT3b-c rectal adenocarcinomas.

As for second-order texture features, energy was significantly higher in pT3a rectal adenocarcinomas than in pT3b-c tumors, while entropy was significantly lower. Theoretically, the meaning of energy is similar to that of uniformity. Entropy represents the spatial disorder of the ADC gray-level distribution. Higher entropy and lower energy reflect greater lesional heterogeneity[35,36]. This may be important when interpreting the findings of second-order textural differences between pT3a and pT3b-c tumors. Similar findings have been reported in previous studies. For example, Caruso *et al*[35] observed significantly higher energy in complete responders compared with non-responders to neoadjuvant chemoradiotherapy for colorectal cancer. In studies exploring the value of ADC texture features in characterizing pathologic features of rectal cancer, pT3-4 rectal cancer was significantly higher in entropy in comparison with pT1-2[33,37].

There were several limitations in the present study. First, because of its retrospective design, selection bias was inevitable. Second, the study population was relatively small, and all patients were enrolled in the same hospital, which indicates the low generalizability of the present findings. The low proportion of ADC from the histogram could not significantly differentiate pT3a from pT3b-c tumors, which contradicted previous studies from our group. A future study would benefit from a larger study population. Third, we did not correlate TA with other MRI sequences such as T2WI. High-resolution T2WI plays a pivotal role in the preoperative staging of rectal cancer. Hence, future studies should include T2WI-based TA. Fourth, although gadolinium was used as the contrast agent for MRI, its effect was not examined in this study. Fifth, the study's outcomes only had short-term clinical applicability. Finally, first- and second-order texture features were derived from the DWI datasets, which are sensitive to the applied  $b$ -values[38]. In designing future studies, the choice of the  $b$ -value needs to be taken into account.

## CONCLUSION

Texture features derived from ADC maps, especially skewness, energy, and entropy, might potentially differentiate pT3a rectal adenocarcinomas from pT3b-c tumors. This could have a practical value for the individualized management of rectal cancer patients.

## ARTICLE HIGHLIGHTS

**Research background**

The accuracy of discriminating pT3a from pT3b-c rectal cancer using high-resolution magnetic resonance imaging remains unsatisfactory. Indeed, the mean and median apparent diffusion coefficient (ADC) values are not always significantly sensitive to small changes or precise status of the tumor owing to the intrinsic chaotic environment of tumors.

**Research motivation**

Texture analysis (TA) could improve the discrimination of pT3a rectal adenocarcinomas from pT3b-c tumors, but pT3 subclasses of rectal cancer have not been previously determined by ADC maps.

**Research objectives**

To investigate the value of TA on ADC maps in differentiating pT3a rectal adenocarcinomas from pT3b-c tumors.

**Research methods**

This case-control study assessed patients with pT3 rectal adenocarcinoma, who underwent DWI between October 2016 and December 2018. First-order (ADC values, skewness, kurtosis, and uniformity) and second-order (energy, entropy, inertia, and correlation) texture features were derived from whole-lesion ADC maps. Receiver operating characteristic (ROC) curves were used to determine the diagnostic value for pT3b-c tumors.

**Research results**

Totally 59 patients (34 men and 25 women) were included, with a median age of 66 years (range, 41-85 years). Thirty patients had pT3a, 24 had pT3b, and five had pT3c. Skewness was significantly lower in the pT3a stage than in pT3b-c tumors. In addition, energy and entropy were significantly different between pT3a rectal adenocarcinomas and pT3b-c tumors. For differentiating pT3a rectal adenocarcinomas from pT3b-c tumors, the areas under the curves (AUCs) of skewness, energy, and entropy were 0.686, 0.657, and 0.747, respectively. Logistic regression analysis of all three features yielded a greater AUC (0.775) in differentiating pT3a rectal adenocarcinomas from pT3b-c tumors (69.0% sensitivity and 83.3% specificity).

**Research conclusions**

TA features derived from ADC maps might potentially differentiate pT3a rectal adenocarcinomas from pT3b-c tumors, especially skewness, energy, and entropy and their combination.

**Research perspectives**

Future studies should include T2WI-based TA, since high-resolution T2WI plays a pivotal role in the preoperative staging of rectal cancer, and *b*-values should also be taken into account. In addition, features with long-term clinical applicability should be assessed. Finally, large multicenter studies are needed to confirm and increase the generalizability of the above findings.

## REFERENCES

- 1 **Bray F**, Ferlay J, Soerjomataram I, Siegel RL, Torre LA, Jemal A. Global cancer statistics 2018: GLOBOCAN estimates of incidence and mortality worldwide for 36 cancers in 185 countries. *CA Cancer J Clin* 2018; **68**: 394-424 [PMID: 30207593 DOI: 10.3322/caac.21492]
- 2 **Kuipers EJ**, Grady WM, Lieberman D, Seufferlein T, Sung JJ, Boelens PG, van de Velde CJ, Watanabe T. Colorectal cancer. *Nat Rev Dis Primers* 2015; **1**: 15065 [PMID: 27189416 DOI: 10.1038/nrdp.2015.65]
- 3 **Glynn-Jones R**, Wyrwicz L, Tiret E, Brown G, Rödel C, Cervantes A, Arnold D; ESMO Guidelines Committee. Rectal cancer: ESMO Clinical Practice Guidelines for diagnosis, treatment and follow-up. *Ann Oncol* 2017; **28**: iv22-iv40 [PMID: 28881920 DOI: 10.1093/annonc/mdx224]
- 4 **Wolf AMD**, Fontham ETH, Church TR, Flowers CR, Guerra CE, LaMonte SJ, Etzioni R, McKenna MT, Oeffinger KC, Shih YT, Walter LC, Andrews KS, Brawley OW, Brooks D, Fedewa SA, Manassaram-Baptiste D, Siegel RL, Wender RC, Smith RA. Colorectal cancer screening for average-

- risk adults: 2018 guideline update from the American Cancer Society. *CA Cancer J Clin* 2018; **68**: 250-281 [PMID: 29846947 DOI: 10.3322/caac.21457]
- 5 **NCCN Clinical Practice Guidelines in Oncology (NCCN Guidelines)**. Rectal Cancer. Version 4.2020. Fort Washington: National Comprehensive Cancer Network. 2020
  - 6 **Zinicola R**, Pedrazzi G, Haboubi N, Nicholls RJ. The degree of extramural spread of T3 rectal cancer: an appeal to the American Joint Committee on Cancer. *Colorectal Dis* 2017; **19**: 8-15 [PMID: 27883254 DOI: 10.1111/codi.13565]
  - 7 **Kaur H**, Choi H, You YN, Rauch GM, Jensen CT, Hou P, Chang GJ, Skibber JM, Ernst RD. MR imaging for preoperative evaluation of primary rectal cancer: practical considerations. *Radiographics* 2012; **32**: 389-409 [PMID: 22411939 DOI: 10.1148/rg.322115122]
  - 8 **Nomura M**, Takahashi H, Fujii M, Miyoshi N, Haraguchi N, Hata T, Matsuda C, Yamamoto H, Mizushima T, Mori M, Doki Y. Clinical significance of invasion distance relative to prognosis in pathological T3 colorectal cancer. *Oncol Lett* 2019; **18**: 5614-5620 [PMID: 31620203 DOI: 10.3892/ol.2019.10913]
  - 9 **Merkel S**, Mansmann U, Siassi M, Papadopoulos T, Hohenberger W, Hermanek P. The prognostic inhomogeneity in pT3 rectal carcinomas. *Int J Colorectal Dis* 2001; **16**: 298-304 [PMID: 11686527 DOI: 10.1007/s003840100309]
  - 10 **Cho SH**, Kim SH, Bae JH, Jang YJ, Kim HJ, Lee D, Park JS; Society of North America (RSNA). Prognostic stratification by extramural depth of tumor invasion of primary rectal cancer based on the Radiological Society of North America proposal. *AJR Am J Roentgenol* 2014; **202**: 1238-1244 [PMID: 24848820 DOI: 10.2214/AJR.13.11311]
  - 11 **Lu ZH**, Hu CH, Qian WX, Cao WH. Preoperative diffusion-weighted imaging value of rectal cancer: preoperative T staging and correlations with histological T stage. *Clin Imaging* 2016; **40**: 563-568 [PMID: 27133705 DOI: 10.1016/j.clinimag.2015.12.006]
  - 12 **Zhong G**, Xiao Y, Zhou W, Pan W, Zhu Q, Zhang J, Jiang Y. Value of endorectal ultrasonography in measuring the extent of mesorectal invasion and substaging of T3 stage rectal cancer. *Oncol Lett* 2017; **14**: 5657-5663 [PMID: 29113193 DOI: 10.3892/ol.2017.6906]
  - 13 **Faletti R**, Gatti M, Arezzo A, Stola S, Benedini MC, Bergamasco L, Morino M, Fonio P. Preoperative staging of rectal cancer using magnetic resonance imaging: comparison with pathological staging. *Minerva Chir* 2018; **73**: 13-19 [PMID: 28497665 DOI: 10.23736/S0026-4733.17.07392-8]
  - 14 **Gillies RJ**, Kinahan PE, Hricak H. Radiomics: Images Are More than Pictures, They Are Data. *Radiology* 2016; **278**: 563-577 [PMID: 26579733 DOI: 10.1148/radiol.2015151169]
  - 15 **Becker AS**, Ghafoor S, Marcon M, Perucho JA, Wurnig MC, Wagner MW, Khong PL, Lee EY, Boss A. MRI texture features may predict differentiation and nodal stage of cervical cancer: a pilot study. *Acta Radiol Open* 2017; **6**: 2058460117729574 [PMID: 29085671 DOI: 10.1177/2058460117729574]
  - 16 **Wibmer A**, Hricak H, Gondo T, Matsumoto K, Veeraraghavan H, Fehr D, Zheng J, Goldman D, Moskowitz C, Fine SW, Reuter VE, Eastham J, Sala E, Vargas HA. Haralick texture analysis of prostate MRI: utility for differentiating non-cancerous prostate from prostate cancer and differentiating prostate cancers with different Gleason scores. *Eur Radiol* 2015; **25**: 2840-2850 [PMID: 25991476 DOI: 10.1007/s00330-015-3701-8]
  - 17 **Ytre-Hauge S**, Dybvik JA, Lundervold A, Salvesen ØO, Krakstad C, Fasmer KE, Werner HM, Ganeshan B, Høivik E, Bjørge L, Trovik J, Haldorsen IS. Preoperative tumor texture analysis on MRI predicts high-risk disease and reduced survival in endometrial cancer. *J Magn Reson Imaging* 2018; **48**: 1637-1647 [PMID: 30102441 DOI: 10.1002/jmri.26184]
  - 18 **Ueno Y**, Forghani B, Forghani R, Dohan A, Zeng XZ, Chamming's F, Arseneau J, Fu L, Gilbert L, Gallix B, Reinhold C. Endometrial Carcinoma: MR Imaging-based Texture Model for Preoperative Risk Stratification-A Preliminary Analysis. *Radiology* 2017; **284**: 748-757 [PMID: 28493790 DOI: 10.1148/radiol.2017161950]
  - 19 **Xu Y**, Xu Q, Ma Y, Duan J, Zhang H, Liu T, Li L, Sun H, Shi K, Xie S, Wang W. Characterizing MRI features of rectal cancers with different KRAS status. *BMC Cancer* 2019; **19**: 1111 [PMID: 31727020 DOI: 10.1186/s12885-019-6341-6]
  - 20 **Oh JE**, Kim MJ, Lee J, Hur BY, Kim B, Kim DY, Baek JY, Chang HJ, Park SC, Oh JH, Cho SA, Sohn DK. Magnetic Resonance-Based Texture Analysis Differentiating KRAS Mutation Status in Rectal Cancer. *Cancer Res Treat* 2020; **52**: 51-59 [PMID: 31096736 DOI: 10.4143/crt.2019.050]
  - 21 **Park H**, Kim KA, Jung JH, Rhie J, Choi SY. MRI features and texture analysis for the early prediction of therapeutic response to neoadjuvant chemoradiotherapy and tumor recurrence of locally advanced rectal cancer. *Eur Radiol* 2020; **30**: 4201-4211 [PMID: 32270317 DOI: 10.1007/s00330-020-06835-4]
  - 22 **Crimi F**, Capelli G, Spolverato G, Bao QR, Florio A, Milite Rossi S, Cecchin D, Albertoni L, Campi C, Pucciarelli S, Stramare R. MRI T2-weighted sequences-based texture analysis (TA) as a predictor of response to neoadjuvant chemo-radiotherapy (nCRT) in patients with locally advanced rectal cancer (LARC). *Radiol Med* 2020; **125**: 1216-1224 [PMID: 32410063 DOI: 10.1007/s11547-020-01215-w]
  - 23 **Tong T**, Yao Z, Xu L, Cai S, Bi R, Xin C, Gu Y, Peng W. Extramural depth of tumor invasion at thin-section MR in rectal cancer: associating with prognostic factors and ADC value. *J Magn Reson Imaging* 2014; **40**: 738-744 [PMID: 24307597 DOI: 10.1002/jmri.24398]
  - 24 **Just N**. Improving tumour heterogeneity MRI assessment with histograms. *Br J Cancer* 2014; **111**: 2205-2213 [PMID: 25268373 DOI: 10.1038/bjc.2014.512]

- 25 **Cortez-Conradis D**, Favila R, Isaac-Olive K, Martinez-Lopez M, Rios C, Roldan-Valadez E. Diagnostic performance of regional DTI-derived tensor metrics in glioblastoma multiforme: simultaneous evaluation of p, q, L, Cl, Cp, Cs, RA, RD, AD, mean diffusivity and fractional anisotropy. *Eur Radiol* 2013; **23**: 1112-1121 [PMID: 23085868 DOI: 10.1007/s00330-012-2688-7]
- 26 **DeLong ER**, DeLong DM, Clarke-Pearson DL. Comparing the areas under two or more correlated receiver operating characteristic curves: a nonparametric approach. *Biometrics* 1988; **44**: 837-845 [PMID: 3203132]
- 27 **Castellano G**, Bonilha L, Li LM, Cendes F. Texture analysis of medical images. *Clin Radiol* 2004; **59**: 1061-1069 [PMID: 15556588 DOI: 10.1016/j.crad.2004.07.008]
- 28 **Srinivasan G**, Shobha G. Statistical texture analysis. *Proc World Acad Sci Eng Technol* 2008; **36**: 1264-1269
- 29 **Kim JH**, Ko ES, Lim Y, Lee KS, Han BK, Ko EY, Hahn SY, Nam SJ. Breast Cancer Heterogeneity: MR Imaging Texture Analysis and Survival Outcomes. *Radiology* 2017; **282**: 665-675 [PMID: 27700229 DOI: 10.1148/radiol.2016160261]
- 30 **Lu Z**, Zhao W, Ji L. The Histogram Analysis of Apparent Diffusion Coefficient Maps with Standard- or Ultrahigh-b Value Diffusion-Weighted MR Imaging for Differentiating the Gleason Grade of Prostate Cancer. *J Med Imaging Health Inf* 2018; **8**: 577-582 [DOI: 10.1166/jmhi.2018.2363]
- 31 **Lu ZH**, Ji LB, Zhao WL, Zhang YS, Wu JF, Li X, Shen JK. Differentiating Transition Zone Cancers From Benign Prostatic Hyperplasia by Histogram Analysis of Apparent Diffusion Coefficient Maps With Standard and Ultrahigh b-value Diffusion-weighted MR Imaging. *J Comput Assist Tomogr* 2019; **43**: 235-241 [PMID: 30475249 DOI: 10.1097/RCT.0000000000000829]
- 32 **Wu CJ**, Wang Q, Li H, Wang XN, Liu XS, Shi HB, Zhang YD. DWI-associated entire-tumor histogram analysis for the differentiation of low-grade prostate cancer from intermediate-high-grade prostate cancer. *Abdom Imaging* 2015; **40**: 3214-3221 [PMID: 26156619 DOI: 10.1007/s00261-015-0499-4]
- 33 **Liu L**, Liu Y, Xu L, Li Z, Lv H, Dong N, Li W, Yang Z, Wang Z, Jin E. Application of texture analysis based on apparent diffusion coefficient maps in discriminating different stages of rectal cancer. *J Magn Reson Imaging* 2017; **45**: 1798-1808 [PMID: 27654307 DOI: 10.1002/jmri.25460]
- 34 **Meng Y**, Zhang C, Zou S, Zhao X, Xu K, Zhang H, Zhou C. MRI texture analysis in predicting treatment response to neoadjuvant chemoradiotherapy in rectal cancer. *Oncotarget* 2018; **9**: 11999-12008 [PMID: 29552288 DOI: 10.18632/oncotarget.23813]
- 35 **Caruso D**, Zerunian M, Ciolina M, de Santis D, Rengo M, Soomro MH, Giunta G, Conforto S, Schmid M, Neri E, Laghi A. Haralick's texture features for the prediction of response to therapy in colorectal cancer: a preliminary study. *Radiol Med* 2018; **123**: 161-167 [PMID: 29119525 DOI: 10.1007/s11547-017-0833-8]
- 36 **Duvaferrier R**, Bezy J, Bertaud V, Toussaint G, Morelli J, Lasbleiz J. Texture analysis software: integration with a radiological workstation. *Stud Health Technol Inform* 2012; **180**: 1030-1034 [PMID: 22874350]
- 37 **Li W**, Jiang Z, Guan Y, Chen Y, Huang X, Liu S, He J, Zhou Z, Ge Y. Whole-lesion Apparent Diffusion Coefficient First- and Second-Order Texture Features for the Characterization of Rectal Cancer Pathological Factors. *J Comput Assist Tomogr* 2018; **42**: 642-647 [PMID: 29613992 DOI: 10.1097/RCT.0000000000000731]
- 38 **Becker AS**, Wagner MW, Wurnig MC, Boss A. Diffusion-weighted imaging of the abdomen: Impact of b-values on texture analysis features. *NMR Biomed* 2017; **30** [PMID: 27898201 DOI: 10.1002/nbm.3669]



Published by **Baishideng Publishing Group Inc**  
7041 Koll Center Parkway, Suite 160, Pleasanton, CA 94566, USA  
**Telephone:** +1-925-3991568  
**E-mail:** [bpgoffice@wjgnet.com](mailto:bpgoffice@wjgnet.com)  
**Help Desk:** <https://www.f6publishing.com/helpdesk>  
<https://www.wjgnet.com>

